

Characterization of surface modification in atomic force microscope-induced nanolithography of oxygen deficient $\text{La}_{0.67}\text{Ba}_{0.33}\text{MnO}_{3-\delta}$ thin films

Cite as: AIP Advances 4, 127129 (2014); <https://doi.org/10.1063/1.4904427>

Submitted: 02 June 2014 • Accepted: 27 November 2014 • Published Online: 16 December 2014

 E. Kevin Tanyi,  Rajeswari M. Kolagani, Parul Srivastava, et al.



View Online



Export Citation



CrossMark

ARTICLES YOU MAY BE INTERESTED IN

[Thin film characterization by atomic force microscopy at ultrasonic frequencies](#)

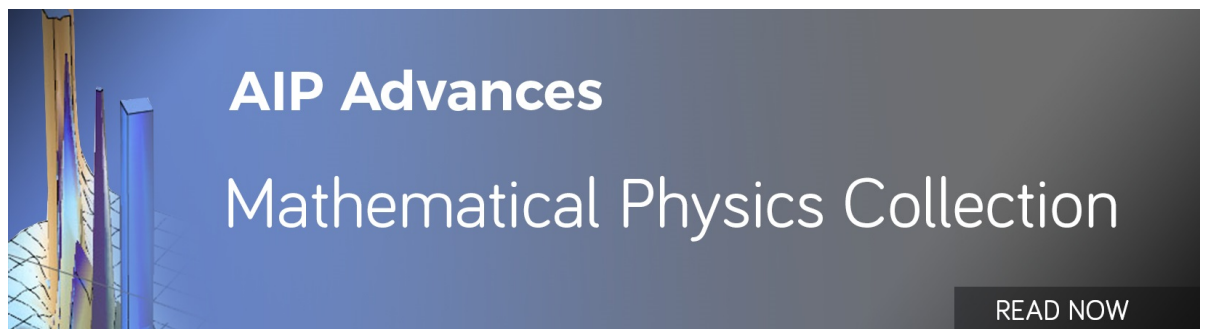
Applied Physics Letters **76**, 1950 (2000); <https://doi.org/10.1063/1.126222>

[Possible mechanisms in atomic force microscope-induced nano-oxidation lithography in epitaxial \$\text{La}_{0.67}\text{Ba}_{0.33}\text{MnO}_{3-\delta}\$ thin films](#)

Journal of Vacuum Science & Technology B **34**, 021601 (2016); <https://doi.org/10.1116/1.4941243>

[Review Article: Stress in thin films and coatings: Current status, challenges, and prospects](#)

Journal of Vacuum Science & Technology A **36**, 020801 (2018); <https://doi.org/10.1116/1.5011790>



AIP Advances
Mathematical Physics Collection

READ NOW

Characterization of surface modification in atomic force microscope-induced nanolithography of oxygen deficient $\text{La}_{0.67}\text{Ba}_{0.33}\text{MnO}_{3-\delta}$ thin films

E. Kevin Tanyi,^{1,a} Rajeswari M. Kolagani,^{1,b} Parul Srivastava,¹
William Vanderlinde,² Grace Yong,¹ Christopher Stumpf,¹
and David Schaefer¹

¹Department of Physics, Astronomy & Geosciences, Towson University, Towson MD 21043, U.S.A

²Laboratory for Physical Sciences, 8050 Greenmead Drive, College Park, MD 20740, U.S.A

(Received 2 June 2014; accepted 27 November 2014; published online 16 December 2014)

We report our studies of the nanolithographic surface modifications induced by an Atomic Force Microscope (AFM) in epitaxial thin films of oxygen deficient Lanthanum Barium Manganese Oxide ($\text{La}_{0.67}\text{Ba}_{0.33}\text{MnO}_{3-\delta}$). The pattern characteristics depend on the tip voltage, tip polarity, voltage duration, tip force, and humidity. We have used Electron Energy Dispersive X-Ray Spectroscopy (EDS) to analyze the chemical changes associated with the surface modifications produced with a negatively biased AFM tip. A significant increase in the oxygen stoichiometry for the patterned regions relative to the pristine film surface is observed. The results also indicate changes in the cation stoichiometry, specifically a decrease in the Lanthanum and Manganese concentrations and an increase in the Barium concentration in the patterned regions. © 2014 Author(s). All article content, except where otherwise noted, is licensed under a Creative Commons Attribution 3.0 Unported License. [<http://dx.doi.org/10.1063/1.4904427>]

I. INTRODUCTION

Nanolithographic surface modification via anodic oxidation has attracted significant interest since 1990, when Dagata et al¹ demonstrated localized oxidation of passivated Silicon (Si) samples using a scanning tunneling microscope (STM). Similar phenomena were also demonstrated using the Atomic Force Microscope (AFM). It has been found that the pattern characteristics such as the height and width are dependent on several parameters such as the electric field (voltage and tip-to-sample distance), humidity, voltage pulse duration, tip speed, and the mode of the AFM operation – i.e. contact mode or tapping mode.^{2–10} Several models including those by Gordon et al,¹¹ Teuschler et al¹² and the Cabrera and Mott¹³ have been proposed to explain the experimental results. In the case of metals such as Ti and Al^{14–16} and semiconductors such as Si;^{2,5} a detailed understanding of the chemical processes associated with STM/AFM-induced nanolithography has been established. AFM induced nanolithographic modification of functional complex metal oxides has attracted some attention in recent years as evidenced by studies on SrTiO_3 ¹⁷, high temperature superconducting materials such $\text{YBa}_2\text{Cu}_3\text{O}_{7-2x}$ ^{18–20} and $\text{HoBa}_2\text{Cu}_3\text{O}_{7-x}$ ²¹ as well as thin films of rare earth manganese oxides exhibiting colossal magnetoresistance and charge ordering.^{22–30} However, unlike in the case of Si and simple metallic systems, there have been no previous efforts to understand the nature of the chemical modifications in the metal oxide materials. Earlier work by Run Wei et al^{22,23} has demonstrated AFM lithography in thin films of $\text{La}_{0.8}\text{Ba}_{0.2}\text{MnO}_3$, focusing on features introduced by positive tip bias ('negative sample voltage' in their terminology) in fully oxygenated samples. Their studies mainly address the morphological characteristics of

^aCurrently at Norfolk State University

^brkolagani@towson.edu (To whom all correspondence should be addressed)

the pattern and etch selectivity resulting from the surface modification. Pallechi *et al.* have employed surface modification induced by an AFM tip to pattern device structures in LBMO films, employing the increase in resistance to obtain resistive barriers.^{25–27} These researchers have demonstrated patterning using negative tip bias in films with different oxygen content, but their focus has been on subsequent field effect studies in the patterned devices by application of external electric field. Yanagisawa *et al.*^{28,29} have used AFM lithography to pattern thin films phase separated $\text{La}_{0.275}\text{Pr}_{0.35}\text{CaMnO}_3$ thin films. They have reported that larger pattern heights can be obtained for oxygen deficient films as compared to oxygen-annealed samples for positive tip bias. The emphasis of their work however, was on changes in the insulator-metal transition temperature and electrical and magneto-resistive properties induced by the surface modification.

In this paper, we report our studies of the AFM-induced nanolithography in an oxygen deficient composition of the colossal magneto-resistive material Lanthanum Barium Manganese oxide ($\text{La}_{0.67}\text{Ba}_{0.33}\text{MnO}_{3-\delta}$), abbreviated as LBMO). In the fully oxygenated state ($\text{La}_{0.67}\text{Ba}_{0.33}\text{MnO}_3$), this material undergoes an insulator-to-metal transition accompanied by ferromagnetic ordering above room temperature and shows colossal magneto-resistance²⁴ which makes it important for potential spintronic devices. For the present study, the LBMO thin films are intentionally fabricated so as to be oxygen deficient since oxygen deficiency may be expected to enhance the effects of anodic oxidation. Oxygen deficient films also have reduced surface roughness which is advantageous for AFM lithography. The study reported here focuses on surface modifications induced by a negatively biased AFM tip which produces large outgrowths. We have analyzed the chemical changes associated with these outgrowths using Electron Energy Dispersive x-ray spectroscopy (EDS).

II. EXPERIMENTAL DETAILS

A. Sample preparation and characterization

The LBMO films were grown on SrTiO_3 (100) (abbreviated as STO) by Pulsed Laser Deposition using a Krypton Fluoride (KrF) laser of wavelength 248 nm and pulse width 20 ns, operated at 10 Hz. The substrate temperature during film growth was 800°C, with laser pulse energy of 450 mJ corresponding to an energy density $\sim 1 \text{ J/cm}^2$ on the target. During film growth an ambient of flowing oxygen was maintained at a partial pressure of 50 mTorr (66.5 μbar) [Note that the oxygen pressure needed for the optimally oxygenated phase is 400 mTorr under our experimental conditions. The oxygen pressure was reduced to achieve oxygen deficient composition in the films for the present study]. The films were cooled down to room temperature in oxygen ambient of $\sim 500 \text{ Torr}$ at a nominal cooling rate of 20 °C/min. The average film thickness was 1,400 Å, the growth rate being 0.14 Å/pulse. The structural properties of the films were characterized using a four circle X-ray diffractometer (Bruker D8 Discover). The results reveal (001) oriented films with good crystalline quality as indicated by a rocking angle (FWHM) of 0.05°. The $2\theta - \omega$ scan of a typical sample is shown in Fig.1 (a). Φ scans (not shown) reveal that the films are in-plane-aligned with a cube-on-cube epitaxial alignment with the substrate. The out of plane lattice constant is determined to be 3.97 Å (in the pseudo-cubic notation). Note that this value of the lattice constant is significantly larger than the c-lattice constant of the fully oxygenated bulk phase, which is 3.90 Å. The expanded c-lattice constant is indicative of the oxygen deficient phase, the expansion resulting from the lattice distortion and the increased Mn^{3+} ion fraction compared to the fully oxygenated phase. Prior to patterning, we characterized the surface morphology of the films using atomic force microscopy. The average roughness (R_a) value obtained for all the samples used was 0.18 nm with a standard deviation of 0.01 nm. It is noteworthy to mention that these films are significantly smoother than the fully oxygenated samples which typically have an order of magnitude higher average surface roughness. This can be understood as resulting from the higher kinetic energy of the adatoms due to the increased mean free path between collisions facilitated by the lower oxygen pressure. Fig.1 (b) shows a representative resistivity versus temperature for the samples in this study. The samples are insulating at room temperature as expected for oxygen deficient samples

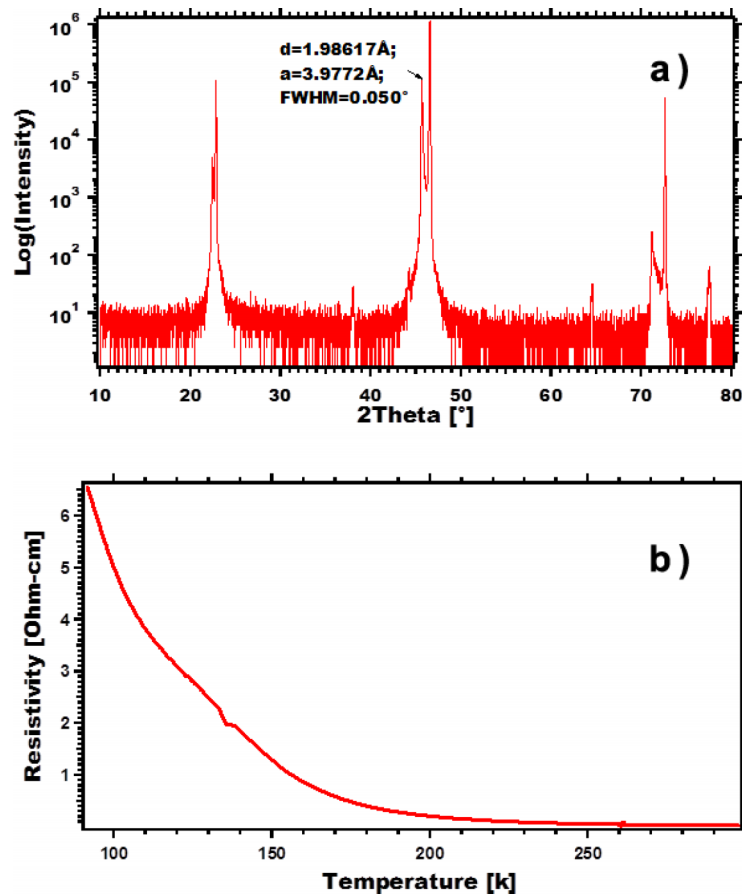


FIG. 1. (a) X-ray Diffraction pattern of the LBMO film. The out-of-plane lattice constant is 3.977 Å (compared to the strain free value of 3.905 Å of an oxygen saturated film). The full width at half max (FWHM) value is 0.050° indicating high crystallinity. The extra peaks (at $2\theta = 38^\circ, 65^\circ, 77^\circ$) are Al peaks from the holder (b) Resistivity versus temperature plot of the LBMO film. The absence of insulator-metal transition and the value of room temperature resistivity are consistent with the oxygen deficiency.

with room temperature resistivity $\sim 0.03\Omega\text{-cm}$, which is about two orders of magnitude higher than that of the fully oxygenated films.

B. Nanolithography experiments

Nanolithography experiments were performed using the AFM mode of a Multimode Nanoscope VII (Veeco) operating in contact mode during both the reading (imaging) and writing (nano-oxidation) processes. Silicon tips plated with Ti/Pt (2/20), with nominal radius of 28 nm and height 12 nm were used in this study. During the nanolithography process, the z-feedback of the AFM controller was employed to maintain a constant force between the tip and the sample, while the x-and y-displacement of the tip was controlled externally by a custom made LabVIEW program. During the nanolithography experiment, the samples were placed in a humidity cell (built in-house) surrounding the AFM tip. The cell was essentially an air tight plastic enclosure with an inlet for nitrogen gas. Prior to passing through the inlet, the nitrogen gas was passed through two beakers; one filled with water to increase the humidity level of the gas and the second beaker to trap any condensed water droplets in the gas.

We performed four separate sets of experiments on each sample, varying the tip voltage and voltage duration. In the first set of experiments designed to investigate the dependence on the tip voltage, we drew lines on the sample 2 to 4 μm apart. The lines were drawn by applying a given

voltage across the tip while moving the tip across the surface in a linear path. As the voltage biased tip is moved across the surface it modifies the surface creating outgrowths that form a line. The voltage bias was then removed and the tip was moved back down to its initial starting position. An offset voltage was then applied to move the tip to a new position on the surface 2 to 4 μm away and the process was repeated to draw the next line. The lines so drawn were 16 μm long. For each line drawn, we recorded the temperature and humidity near the sample surface. The results reported here were obtained at an average relative humidity of $\sim 75\%$. The lowest humidity needed to obtain any surface modification was 61% and the maximum attainable relative humidity was 85%.

During a second set of experiments, while holding the tip at a fixed position above the sample, we applied voltage pulses of varying magnitude and sign for varying time durations, details of which are discussed in the next section. We then moved the tip to a new spot 2-4 μm away and repeated the process, successively increasing the duration of the voltage pulse. This process created 'dots' whose height and width characteristics were dependent on the time duration, with all the other parameters held constant. From the height and width data thus obtained, a growth rate was established.

C. Chemical analysis using energy dispersive x-ray spectroscopy (EDS)

Chemical analysis of the sample surface was performed in a LEO 1550 FE scanning electron microscope equipped with a Thermo Scientific NORAN System 7 X-ray microanalysis system with a 60 mm^2 area silicon drift detector (SDD). In EDS, the sample is bombarded with electrons to knock out core electrons thus stimulating the emission of characteristic X-rays from the specimen. The limitations of EDS for thin film analysis must be kept in mind as the X-rays typically originate from a depth of up to a micron in the sample, resulting in limited spatial resolution. Hence for thin films, care must be taken to avoid measuring x-rays from the underlying substrate. This limitation is particularly serious when analyzing oxygen stoichiometry in metal oxide thin films when the substrates are also oxides. It can also affect the analysis of cation stoichiometry when the film and the substrate contain same cations. The attenuation depth for the electron beam depends on the electron energy, the material being analyzed, and the tilt of the sample, and can be modelled using Monte Carlo simulation methods. Such simulations have shown that it is possible to get reliable results from thin film layers 100 nm or less in thickness by using low electron beam energy of 5 keV.³¹ We have performed simulations for LBMO thin films on SrTiO_3 to identify suitable energies for our film thickness. The details are discussed in the following section.

III. RESULTS AND DISCUSSION

A. Voltage polarity and magnitude dependence of nanolithography characteristics

With a positive tip bias relative to the sample, we were consistently able to draw well defined and reproducible line patterns, the threshold voltage for line formation being 5V. In Fig. 2 (a) and Fig. 2 (b) we show lines drawn with positive tip voltage in the range 1 V to 10 V and 11 V to 20 V respectively, using write speeds of 1.6 $\mu\text{m}/\text{s}$. The widths of these structures were generally between 0.3 μm to 1.5 μm . We were able to control the widths by choosing a moderate voltage below 10 V and adjusting the writing speed, indicating the potential for fabrication of sub-micron features in LBMO films using AFM lithography.

Interestingly, reversing the voltage polarity, (i.e. with tip negatively biased with respect to the sample) produced remarkably different results for the same write speed of 1.6 $\mu\text{m}/\text{s}$. The threshold voltage for line formation in this case is generally found to be between -9 V and -11V, with the -9V threshold occurring most frequently. In Fig. 3 (a) we show the pattern observed while varying the voltage from -11 V to -20 V with a write speed set at 1.6 $\mu\text{m}/\text{s}$. We found that at these higher voltages, excessive outgrowths occur, which prevent the tip from moving, resulting in the formation of a large laterally extending feature instead of well separated lines. However, by increasing the write speed to 16 $\mu\text{m}/\text{s}$ and the line spacing from 2 μm to 4 μm , we were capable of writing controllable and reproducible lines with voltages ~ -15 V, as shown in Fig.3 (b).

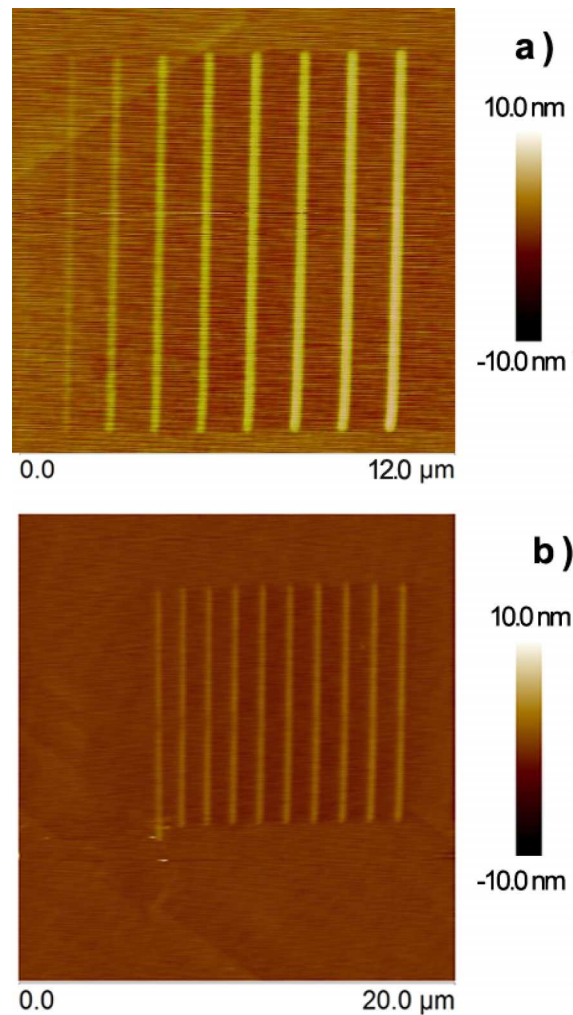


FIG. 2. (a) Lines created using a tip voltage of +1 V to +10 V at a write speed of 1.6 $\mu\text{m/s}$ (b) Lines created using a tip voltage of +11 V to +20 V at a write speed of 1.6 $\mu\text{m/s}$.

The voltage polarity dependence we observe in the oxygen deficient ($\text{La}_{0.7}\text{Ba}_{0.3}\text{MnO}_{3-\delta}$) films is qualitatively similar to that observed by Liu *et al* in post-annealed $\text{La}_{0.8}\text{Ba}_{0.2}\text{MnO}_3$ films,²³ the negative tip bias resulting in more pronounced surface modification. This may be understood as related to the fact that negative tip bias (equivalent to positive sample bias as denoted by Liu *et al*) drive OH^{-1} ions to the sample surface resulting in anodic oxidation which may result in outgrowths. However, it is noteworthy that writing is possible even with the opposite polarity, which suggests that there are other electrochemical processes at work in addition to anodic oxidation. Such processes involving cation stoichiometry changes are borne out in our EDS analysis presented in the next section.

We have investigated the dependence of the line height on the magnitude of the tip bias voltage for both voltage polarities. As shown in Fig.4, line height increases with positive tip voltage. A slight plateau is observed between 10 V and 12 V. It is possible that the plateau region may be separating the two different voltage regimes distinguished by different physical/chemical processes involved in the formation of the pattern. When the same experiment was repeated with a negative tip voltage, we obtained a similar dependence of the line height on the tip voltage (as is also shown in Fig.4). However, the line height obtained with a negative bias was generally higher than that obtained with a positive tip bias of the same magnitude. This suggests a polarity dependent difference in the surface modification indicative of electrolytic processes. As in the case of lines,

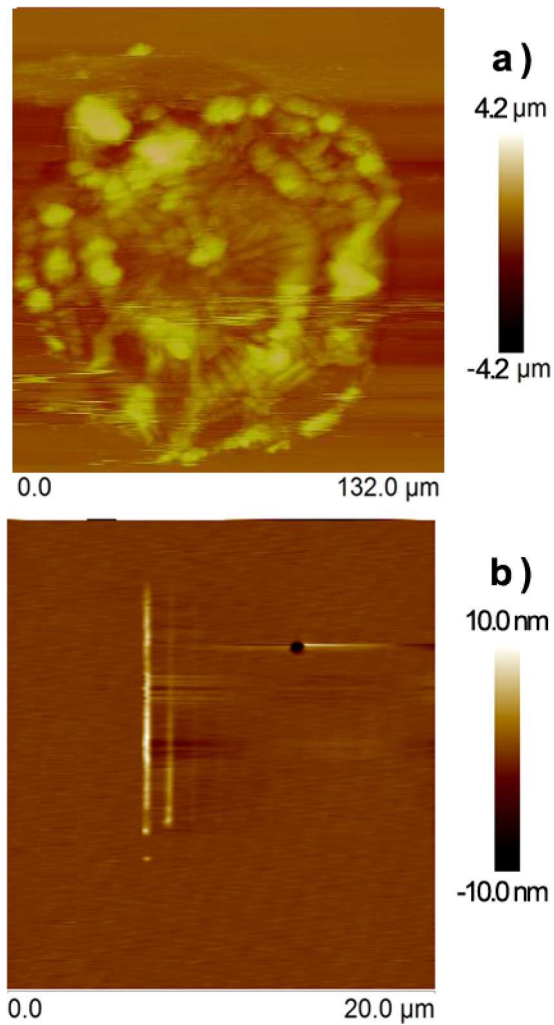


FIG. 3. (a) Uncontrolled growth pattern observed using a tip voltage of -20 V to -11 V at a write speed of 1.6 $\mu\text{m/s}$. (Temperature=85.6°F and relative humidity = 72%) (b) Lines created using a tip voltage of -15 V to -6 V at a write speed of 16.0 $\mu\text{m/s}$. (Temperature= 88.2 °F and relative humidity = 66 %). The voltage threshold for this particular area of the film was around -11 V.

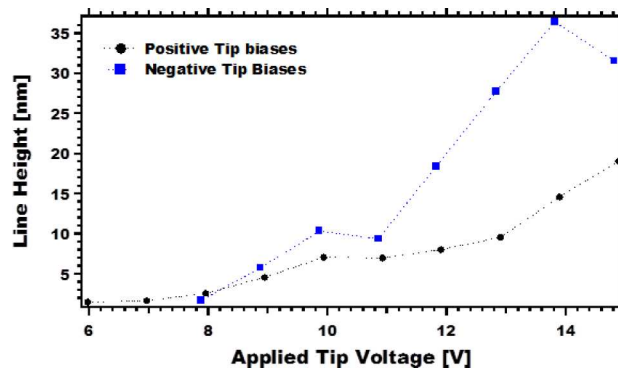


FIG. 4. Line heights created by varying the bias polarities and voltages. The negative voltages clearly show much larger features than those generated by the positive voltages.

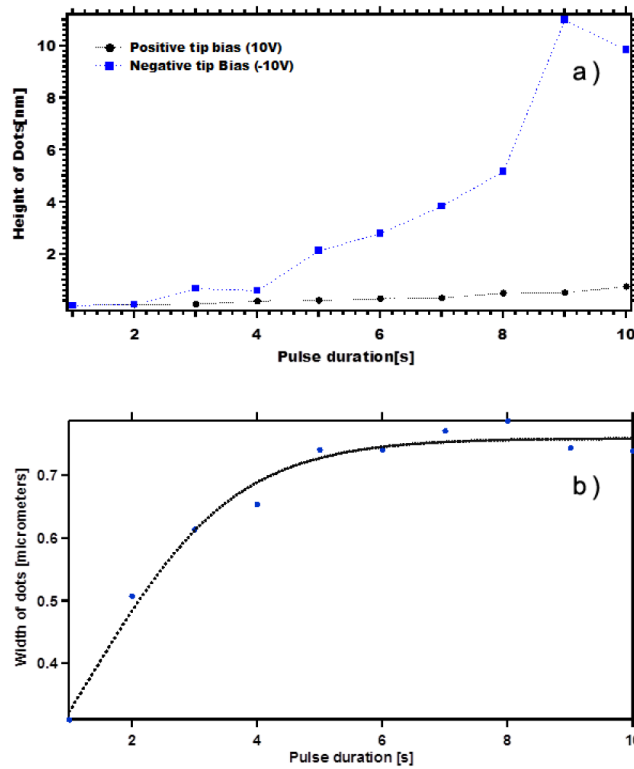


FIG. 5. (a) Comparison of the height of the dots produced at 10 V for various durations of a voltage pulse. Once again, the negative voltage biases produce the highest features (b) Variation of the width of the dots produced at -10 V with the duration of the pulse. The widths saturate after a duration of ~ 5 seconds.

we found a large difference between the heights of ‘dots’ created with a positive tip voltage of 10V from those created with a negative tip voltage of -10 V, the latter being an order of magnitude larger for the same duration of the voltage pulse, as shown in Fig.5(a). The negative tip voltage pulse once again created higher features. Fig.5(b) shows a plot of the width of the dots produced with a negative tip voltage versus the voltage pulse duration for a -10 V voltage pulse. The width

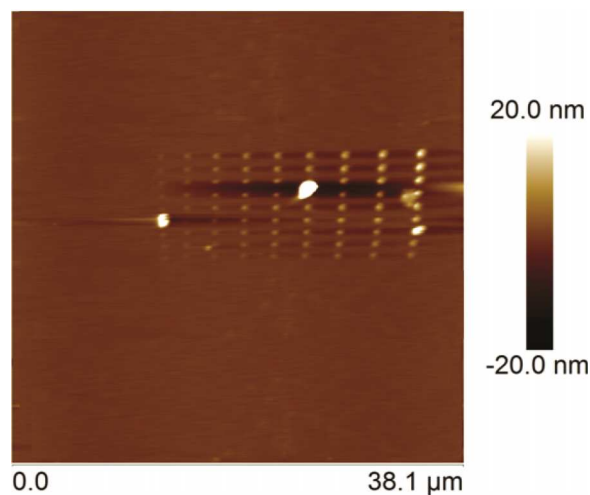


FIG. 6. This is a matrix of dots drawn by varying the duration of the -10 V pulse from 1 s (left- most column) to 10 s (right-most column).

initially increases linearly with time and saturates after ~ 5 seconds. A matrix of dots patterned by this process is shown in Fig.6, with widths in the range $1.2 \mu\text{m}$ to $1.4 \mu\text{m}$. We were able to get sub-micron dots with negative tip voltage pulses with pulse duration of about 0.001 to 0.1 seconds, indicating potential for a fast writing process.

Another interesting result in our studies is the observation of lateral growth patterns associated with lines that extended far beyond the tip or cantilever dimensions. The dendritic lateral growth features shown in Fig. 7(a) occur under high humidity conditions ($\sim 80\%$) with positive tip voltages and slow write speeds. These dendritic growths originating from the patterned lines may signal solid state diffusion under the influence of the electric field due to bias voltage which could be strong enough to create local ion movement. A different type of lateral growth is observed for high negative tip bias (-15V), which is shown in Fig.7 (b). This growth pattern was observed to extend from a newly formed uncontrolled growth structure to an already existing one. The “spark-like growth” formed may be an indication that the oxide formed in the area of uncontrolled growth may be charged or it may have created local stresses that affected the mobility of the ions in the film around it producing a lateral directional growth.

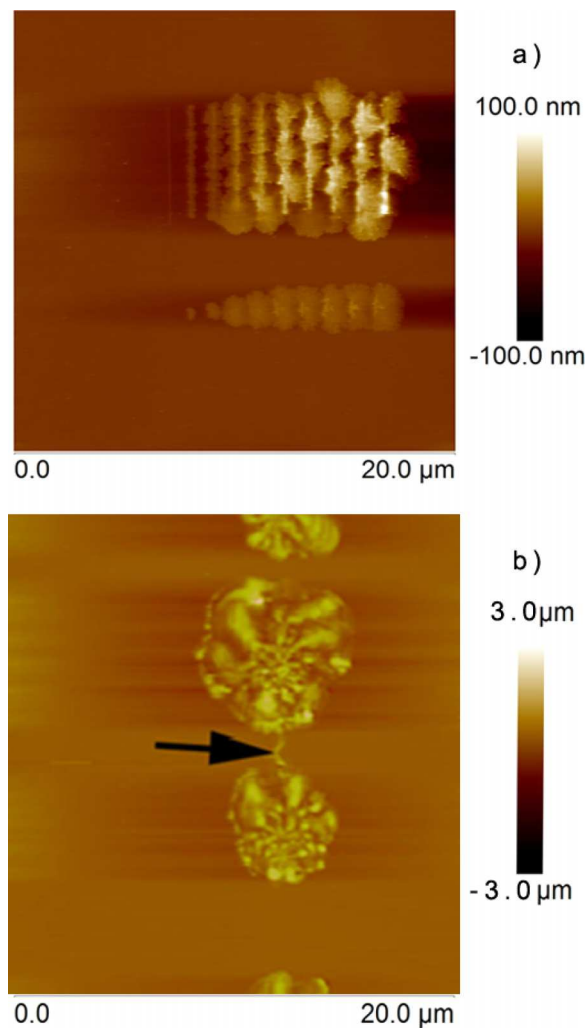


FIG. 7. (a) A “dot-dash-line pattern” obtained using positive tip voltages ranging from 6 V to 15 V while using long time delays of 500 ms (i.e. slow write speeds) and at a high humidity level (80 % relative humidity). Note the dendritic lateral outgrowths originating from the patterns drawn (b) Lateral growth bridging neighboring circular outgrowths formed at high negative tip bias. These lateral growths appear to be directional.

B. SEM/EDS analysis

We have employed elemental analysis using Energy Dispersive X-ray Spectroscopy (EDS) to investigate chemical changes associated with the large outgrowths produced by the negatively biased AFM tip. Images of the patterned lines were also recorded using the scanning electron microscope (SEM). SEM images of lines that were produced using a negative tip bias at varying line speeds are shown in Fig. 8(a). The trench visible in the middle of each line is as a result of abrasion as the oxide grows higher than the z-feedback limit of the AFM. This image clearly shows that the pattern produced does affect regions further away from the tip, indicating that the material used to form the growth pattern is pulled from neighboring regions. Fig. 8(b) shows a larger area that was patterned using negative tip bias, which produces lines at low voltages and the uncontrollable outgrowths at higher voltages, as mentioned earlier. This SEM image also includes some dot patterns. The dot patterns were produced with voltages greater than -15 V, which cause the dots to grow very fast. The smallest dot was produced with a voltage pulse of about 10 s. The SEM image in Fig. 8(c) is a magnified version of the edge of one of the large dots in Fig. 8(b), showing cracks

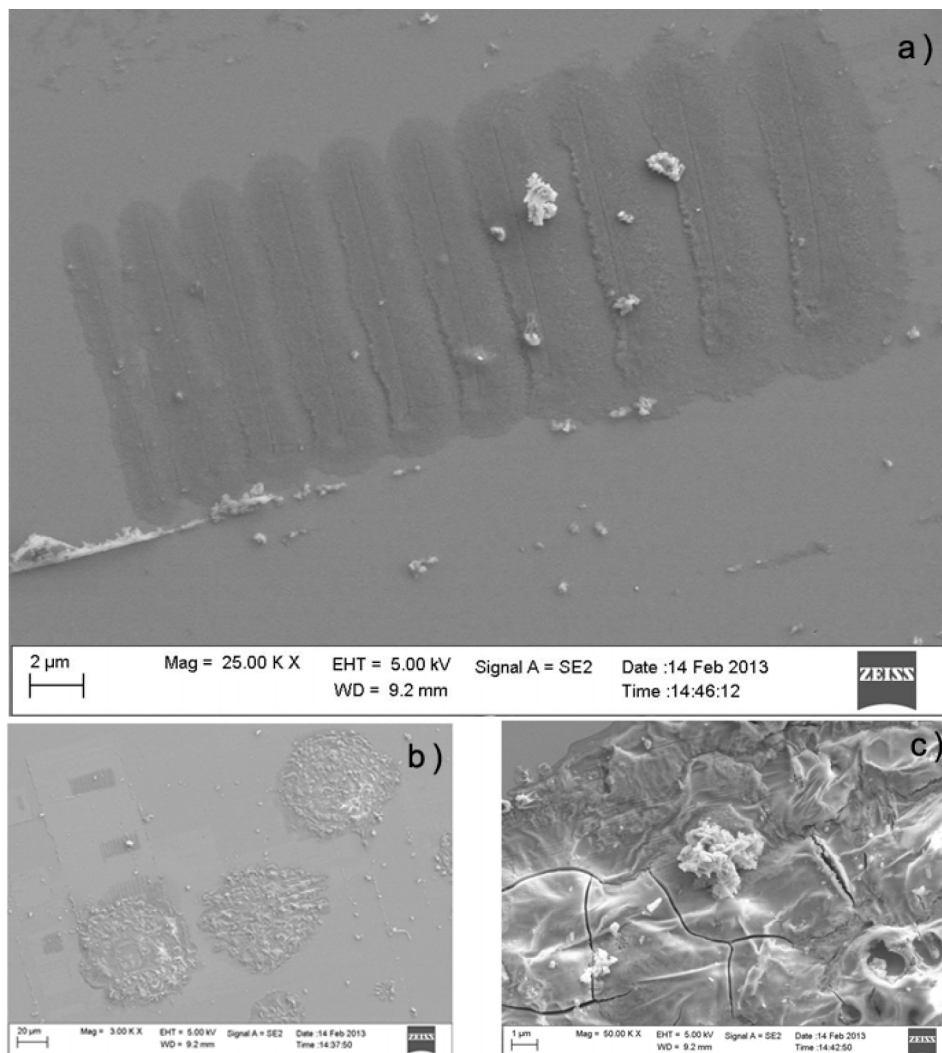


FIG. 8. (a) SEM image of the line patterns produced with a negatively biased voltage at varying line speeds. The trench visible in the middle of each line is as a result of abrasion as the oxide grows higher than the z-feedback limit (b) Dot patterns produced with voltages greater than -15 V (c) Magnified version of the edge of one of the large dots shown in figure 8(b), indicating cracks within the oxide that forms the pattern.

within the material that forms the pattern. We believe that these cracks may be the result of stresses due to localized changes in the crystal structure accompanying oxidation or cationic diffusion. The huge extent of the lateral growth of the patterns formed with negative voltages greater than -15 V may be associated with the trapping of moisture in these cracks, which promotes the propagation of the oxidation reaction. In other words, the oxide formed using a negatively biased tip is not self-limiting.

We have examined the chemical composition in these patterned regions as compared to the stoichiometry of the pristine regions. The EDS analysis has been carried out on patterns produced by negative tip voltages, which represent the largest feature size observed. As mentioned in the experimental section, while investigating oxygen stoichiometry changes, it is important to keep the electron energy low enough to exclude contributions from the SrTiO_3 substrate. To ensure that our EDS signals arise from the film, we have performed Monte Carlo simulation of the electron trajectories and x-ray emission from a 140 nm LBMO thin film on a STO substrate at a beam energy of 5 KeV. The simulation was performed using the DTSA-II software package.³² The result shown in Fig.9 indicates that the oxygen X-rays produced by the 5 KeV originate almost entirely from the LBMO film which is 140 nm thick. Fig.10 shows the EDS spectra obtained at 5 KeV beam energy from the line regions obtained at low negative tip bias [Fig 8(a)]. The corresponding elemental compositions are listed in Table-I. Table II lists elemental compositions from EDS spectrum (not shown) of the circular regions obtained for tip bias > 15 V[Fig. 8(b)]. The oxygen content changes from 19.5 weight% in the pristine regions to 23.5 weight % inside the line pattern, and to 26.8 weight % inside the circular pattern. This indicates progressive increase in oxygen content with increasing AFM tip bias. The observed increases of ~ 3.5 to 7.3 weight % is large enough to be qualitatively sound. The increase in oxygen content is consistent with the fact that negative tip bias is expected to drive the OH⁻ ions towards the sample leading to the oxidation of the region beneath the tip. Note that the 5 KeV EDS spectra are not reliable for determining cation ratios due to the overlap of La and Ba peaks.

To investigate possible cation stoichiometry changes, we obtained EDS spectra at 12 keV (shown in Fig.11) since La and Ba peaks overlap at lower energies. The cation compositions obtained from this data are summarized in Table III. Although we do expect to have x-ray signals from the substrate at this energy, this does not present a problem for the cation stoichiometry analysis since there are no common cations between the film and the substrate. The cation stoichiometry in the pristine regions agrees closely with the expected composition based on the stoichiometry of the PLD target. Interestingly, spectra from the regions modified by the negatively biased AFM tip

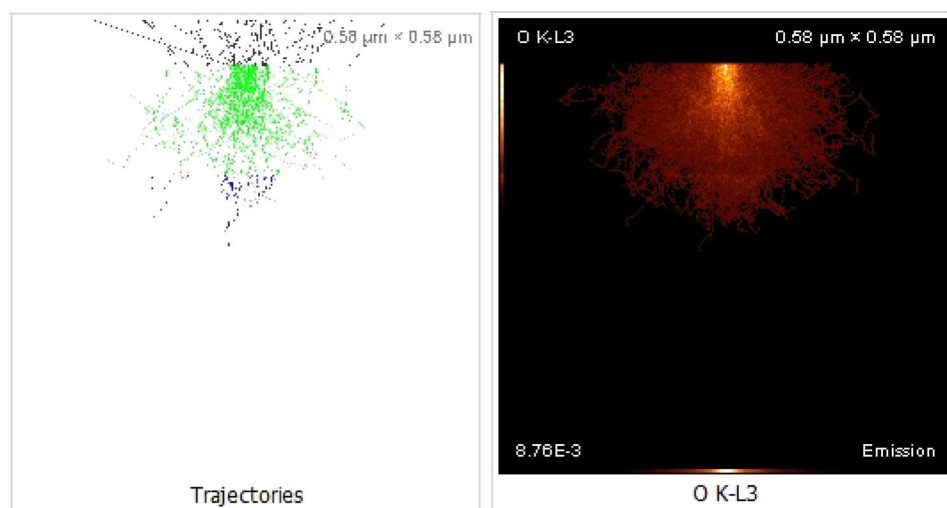


FIG. 9. Monte Carlo simulation of electron trajectories and x-ray emission from a 140nm LaBaMnO₃ thin film on a STO substrate at 5KeV beam energy. Almost all of the oxygen X-rays originate from the LaBaMnO₃ film.

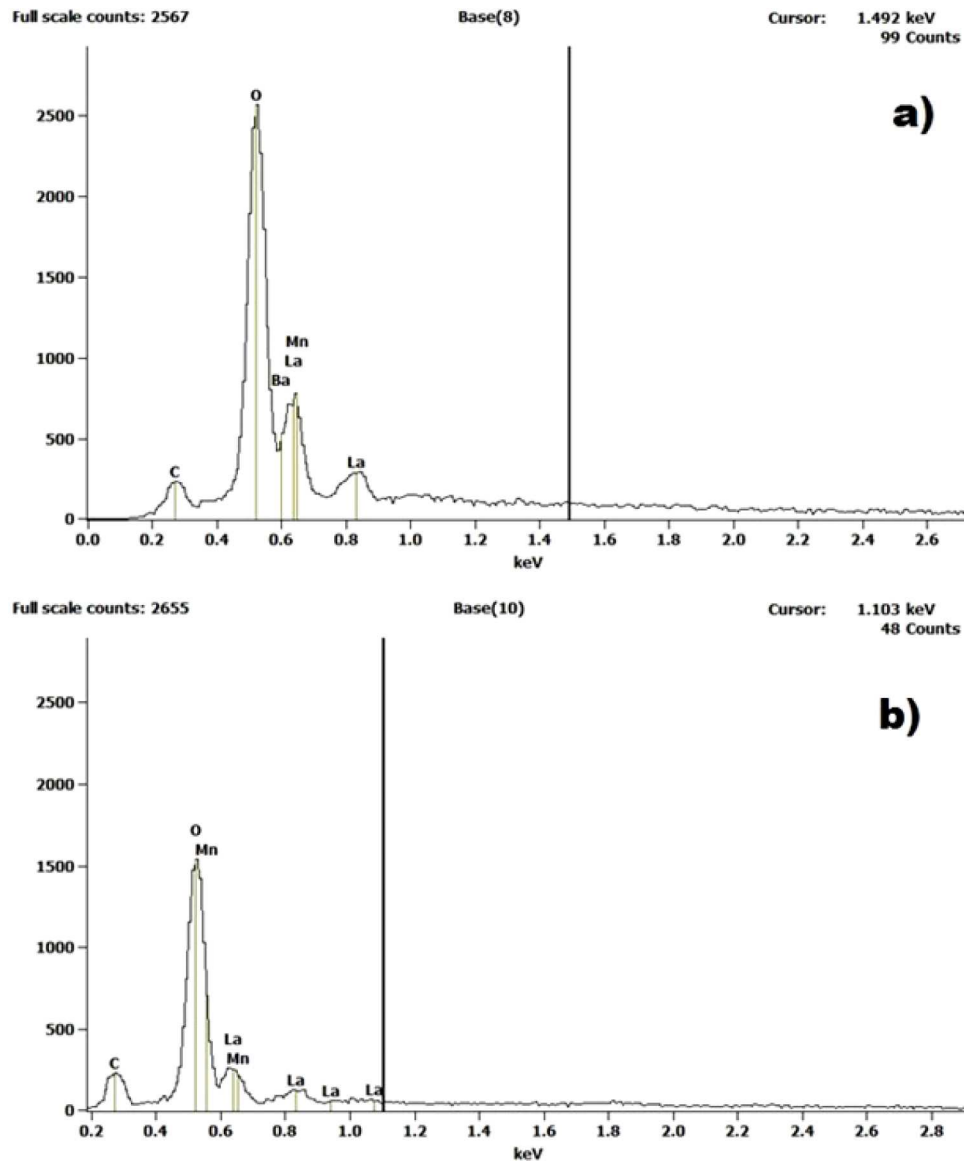


FIG. 10. Energy Dispersive X-ray Spectra (EDS) of LBMO obtained with a 5 keV electron beam. (a) EDS Spectrum from a pristine unmodified region of the sample (b) EDS Spectrum from a sample modified by AFM lithography with a negatively biased tip.

TABLE I. Comparison of the oxygen stoichiometry of a pristine region in the sample to the oxygen stoichiometry in the region modified by a negative tip voltage using EDS data obtained with an electron beam energy of 5 KeV. The area analyzed is one of the lines shown in Fig.8(a). Note that the cation composition cannot be resolved at 5 KeV.

Element– X-ray Line	Weight % : Pristine Region	Weight % : Modified Region	Change in weight %: Modified Region	% Change
C-K	3.1	4.9	1.8	58.1
O-K	19.5	23.0	3.5	17.9
Mn-L	46.6	47.3	0.70	1.5
La-L	30.9	24.8	-6.1	-19.7

TABLE II. Comparison of the oxygen stoichiometry of a pristine region in the sample to the oxygen stoichiometry in the region modified by a negative tip voltage using EDS data obtained with an electron beam energy of 5 KeV. The area analyzed is one of the dots shown in Fig.8(b). Note that the cation composition cannot be resolved at 5 KeV.

Element– X-ray Line	Weight % : Pristine Region	Weight % : Modified Region	Change in weight %: Modified Region	% Change
C-K	3.1	6.5	3.4	109.4
O-K	19.5	26.8	7.3	37.6
Mn-K	46.6	41.4	-5.2	-11.2
La-L	30.9	25.3	-5.6	-18.2

reveal changes in the La to Ba ratio, corresponding to a Ba rich composition in these regions. This suggests ionic diffusion during the patterning process under the influence of electric field gradients, consistent with the lateral outgrowths described earlier. Also, we observe a reduction of Mn content in the patterned areas.

It is also important to note that the substrate composition is also affected as shown by the drop in the Ti and Sr concentrations. These results were consistent with some etching experiments we have carried out indicating that chemical modifications extend into the surface layers of the substrate. In order to understand the chemical mechanisms behind the observed changes calls for further experiments which we are currently working on.

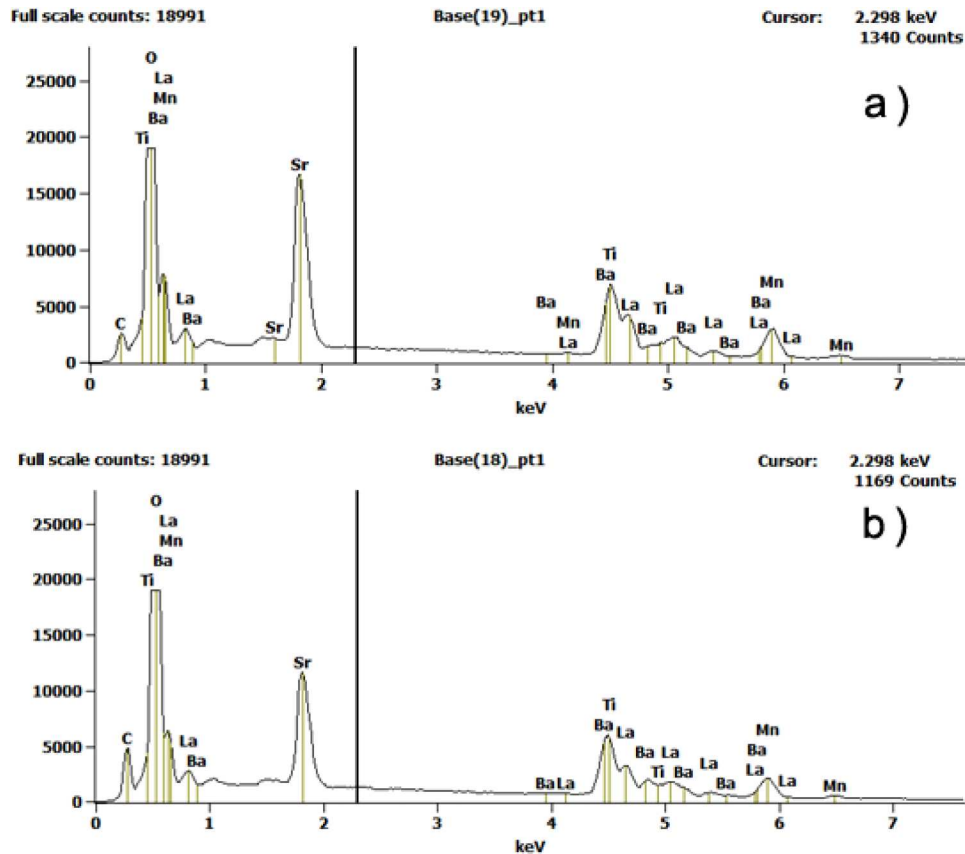


FIG. 11. Energy Dispersive X-ray Spectra (EDS) of LBMO obtained with a 12 keV electron beam. (a) EDS Spectrum from a pristine unmodified region of the sample (b) EDS Spectrum from a sample modified by AFM lithography with a negatively biased tip.

TABLE III. Comparison of the cationic composition of the as-grown film to the composition in the area modified by a negative tip voltage, from EDS data obtained with an electron beam energy of 12 KeV. The modified area analyzed is the 'dot' area shown in Fig.8(b).

Element– X-ray Line	Weight % : Pristine Region	Weight % : Modified Region	Change in Weight %: Modified Region	% Change
C-K	4.0	6.5	2.5	62.5
O-K	19.6	24.8	5.2	26.5
Ti-K	10.4	6.4	-4	-38.5
Mn-K	12.2	9.4	-2.8	-22.9
Sr-L	16.5	12.0	-4.5	-27.3
Ba-L	11.6	19.7	8.1	69.8
La-L	25.7	21.2	-4.5	17.5

IV. CONCLUSIONS

We have demonstrated AFM induced patterning of sub-micron features in oxygen deficient LBMO thin films and characterized the dependence of these features on the polarity and magnitude of the tip bias voltage. We observe that with negative tip voltages, the characteristics of the pattern formation is very sensitive to the write speeds, higher speeds being more conducive to controllable fabrication of sub-micron structures as we have demonstrated for speeds of 16 $\mu\text{m/s}$ where we are able to pattern features sizes ~ 0.3 to 1.5 μm . Compositional analysis shows increase in the weight % of oxygen in the regions patterned with negative tip bias. Cationic composition also shows changes with the patterned regions showing a Ba-rich stoichiometric composition. Thus the surface modification appears to be a composite effect of anodic oxidation and changes in cation stoichiometry.

ACKNOWLEDGMENT

This work was partially supported by the NSF grant ECCS 1128586.

- ¹ J. A. Dagata, J. Schneur, H. H. Harary, C. J. Evans, M. T. Postek, and J. Bennett, *Appl. Phys. Lett.* **56**, 2001 (1990).
- ² P. Avouris, T. Hertel, and R. Martel, *Appl. Phys. Lett.* **71**, 285 (1997).
- ³ Y. Okada, Y. Luchi, M. Kawabe, and J. S. Harris, *J. Appl. Phys.* **88**, 1136 (2000).
- ⁴ K. Wilder, C. F. Quate, D. Adderton, R. Bernstein, and V. Elings, *Appl. Phys. Lett.* **73**, 2527 (1998).
- ⁵ M. Tello and R. Garcia, *Appl. Phys. Lett.* **79**, 03 (2001).
- ⁶ K. Hu, S. Wu, M. Huang, X. Hu, and Q. Wang, *Ultramicroscopy* **115**, 07 (2012).
- ⁷ A. M. Abdullah, S. D. Hutagalung, and Z. Lockman, *Int. J. Nanosci.* **09**, 251 (2010).
- ⁸ B. Garipcan, J. Winters, J. S. Atchison, M. D. Cathell, J. D. Schiffman, O. D. Leaffer, S. S. Nonnenmann, C. L. Schauer, E. Pişkin, B. Nabet, and J. E. Spanier, *Langmuir* **24**(16), 8944–8949 (2008).
- ⁹ M Bartošík, D Skoda, O Tomanec, R Kalousek, P Jánký, J Zlámál, J Spousta, and T Sikola, *J. Phys. Conference Series* **61** (2007).
- ¹⁰ A. Dehhangi, F. Larki, S. D. Hutagalung, M. G. Naseri, B. Y. Majlis, M. Navasery, N. A. Hamid, and M. Mo. Noor, *PLOS ONE* **8**(6), (2013).
- ¹¹ A. E. Gordon, R. T. Fayfield, D. D. Litfin, and T. K. Higman, *J. Vac. Sci. Technol.* **B13**, 2805 (1995).
- ¹² T. Teuschler, K. Mahr, S. Miyazaki, M. Hundhausen, and L. Ley, *Appl. Phys. Lett.* **67**, 3144 (1995).
- ¹³ N. Cabrera and N. F. Mott, *Rep. Prog. Phys.* **12**, 163 (1949).
- ¹⁴ B. Irmer, M. Kehrle, H. Lorenz, and J. P. Kotthaus, *Appl. Phys. Lett.* **71**, 1733 (1997).
- ¹⁵ E. S. Snow and P. M. Campbell, *Science* **270**, 1639 (1995).
- ¹⁶ H. Sugimura, T. Uchida, N. Kitamura, and H. Masuhara, *J. Phys. Chem.* **98**, 4352 (1994).
- ¹⁷ L. Pellegrino, D. Marrè, E. Bellingeri, and A. S. Siri, *Appl. Phys. Lett.* **81**, 3849 (2002).
- ¹⁸ S. C. Wimbush, M. Tachiki, E. Takayama-Muromachi, and H. Itozaki, *Jpn. J. Appl. Phys.* **45**, 5742 (2006).
- ¹⁹ Li-Xing You, Xiao-Bo Yin, Yi-Jun Feng, Sen-Zu Yang, Lin Kang, Wang Mu, and Pei-Heng Wu, *Chinese Phys. Lett.* **19**, 854 (2002).
- ²⁰ G. Bertsche, W. Clauss, and D. P. Kern, *Appl. Phys. Lett.* **68**, 3632 (1996).
- ²¹ H. Heinzelmann, D. Anselmetti, R. Wiesendanger, H. J. Güntherodt, E. Kaldis, and A. Wisard, *Appl. Phys. Lett.* **53**, 2447 (1988).
- ²² R. Wei Li, T. Kanki, H.-A. Tohyami, J. Zhang, H. K. Tanaka, A. Takagi, T. Matsumoto, and T. Kawai, *J. Appl. Phys.* **95**, 7091 (2004).
- ²³ R. Wei Li, T. Kanki, H.-A. Tohyami, J. Zhang, H. K. Tanaka, A. Takagi, T. Matsumoto, and T. Kawai, *Int. J. Nanotechnol.* **6**(12), 1067 (2009).

- ²⁴ R.-W. Li, T. Kanki, H.-A. Tohyama, M. Hirooka, H. Tanaka, and T. Kawai, *Nanotechnology* **16**, 28–31 (2005).
- ²⁵ M. Hirooka, Y. Yanagisawa, T. Kanki, H. Tanaka, and T. Kawai, *Appl. Phys. Lett.* **89**, 163113 (2006).
- ²⁶ I. Pallecchi, L. Pellegrino, E. Bellingeri, A. S. Siri, and D. Marré, *Appl. Phys. Letts.* **83**(21), 4435–4437 (2003).
- ²⁷ I. Pallecchi, L. Pellegrino, E. Bellingeri, A. S. Siri, and D. Marré, *J. Appl. Phys.* **95**(12), 8079–8086 (2004).
- ²⁸ Y. Yanagisawa, H. Tanaka, T. Kawai, and L. Pellegrino, *J. Appl. Phys.* **100**, 124316 (2006).
- ²⁹ Y. Yanagisawa, H. Tanaka, T. Kawai, and L. Pellegrino, *Appl. Phys. Lett.* **89**, 253121 (2006).
- ³⁰ C.N.R Rao and B. Raveau (Eds.), in *Colossal Magnetoresistance, Charge Ordering and Related Properties of Manganese Oxides* (World Scientific Publishing Co, 1998).
- ³¹ W. E. Vanderlinde and D. Chernoff, *Proceedings of the 31st International Symposium for Testing and Failure Analysis*, pp. 370-379 (2005).
- ³² <http://www.cstl.nist.gov/div837/837.02/epq/dtsa2/>.